

An Real-Sim-Real (RSR) Loop Framework for Generalizable Robotic Policy Transfer with Differentiable Simulation

Lu Shi¹, Yuxuan Xu², Shiyu Wang², Jinhao Huang¹, Wenhao Zhao³,
Zike Yan¹, Weibin Gu¹, and Guyue Zhou¹

Abstract—The sim-to-real gap remains a critical challenge in robotics, hindering the deployment of algorithms trained in simulation to real-world systems. This paper introduces a novel Real-Sim-Real (RSR) loop framework leveraging differentiable simulation to address this gap by iteratively refining simulation parameters, aligning them with real-world conditions, and enabling robust and efficient policy transfer. A key contribution of our work is the design of an informative cost function that encourages the collection of diverse and representative real-world data, minimizing bias and maximizing the utility of each data point for simulation refinement. This cost function integrates seamlessly into existing reinforcement learning algorithms (e.g., PPO, SAC) and ensures a balanced exploration of critical regions in the real domain. Furthermore, our approach is implemented on the versatile Mujoco MJX platform, and our framework is compatible with a wide range of robotic systems. Experimental results on several robotic manipulation tasks demonstrate that our method significantly reduces the sim-to-real gap, achieving high task performance and generalizability across diverse scenarios of both explicit and implicit environmental uncertainties. Please refer to our GitHub repository <https://github.com/sunnyshi0310/RSR-MJX.git> for the code.

I. INTRODUCTION

In recent years, simulation has become an indispensable tool in the field of robot learning, especially for developing and testing intelligent control algorithms [1]. The use of simulations allows researchers to train policies in a safe and cost-effective environment, avoiding the risks associated with physical robots, such as damage to the robot or the surrounding environment. In addition, simulation enables rapid experimentation, which is critical in reducing the time and data costs required to train machine learning models.

The sim2real gap refers to the discrepancies between the simulated environment and the real world [2], [3]. While simulation provides a high level of control over the training process, the virtual environment often does not capture the full complexity and variability of the real world. As a result, policies trained in simulation may not generalize well when applied to real robots, leading to suboptimal or unsafe behavior [4]. Sim2real gap may arise from various sources, especially differences in physics, sensor noise, and environmental uncertainties.

The authors are with ¹Institute for AI Industry Research (AIR), Tsinghua University, ² Beijing Jiaotong University, and ³The Hong Kong University of Science and Technology (Guangzhou).

We gratefully acknowledge the support of Wuxi Research Institute of Applied Technologies, Tsinghua University under Grant 20242001120 and the Shuimu Scholarship of Tsinghua University. Any opinions, findings and conclusions or recommendations expressed in this material are those of the authors and do not necessarily reflect the views of the funding agencies.

Various approaches have been proposed to address these challenges [5]. One of the most widely used techniques is Domain Randomization (DR) [6]. DR enhances generalization by increasing the diversity of the simulated environment, training algorithms across a wide range of parameter variations. Although effective, DR often requires manual selection of parameters to randomize, lacks scalability as the complexity of the problem grows, and operates as an open-loop approach that does not incorporate feedback from real-world data. Another promising avenue lies in domain adaptation [7], where the sim2real problem is framed as a transfer learning task. In this paradigm, the simulation domain (source domain) and the real world domain (target domain) are bridged through feature alignment techniques, such as adversarial methods [8] or reconstruction-based approaches [9]. Despite their success in computer vision, adapting these methods to robotics poses unique challenges, particularly in extracting and leveraging invariant features for domain matching and transfer. Additionally, techniques such as neural-augmented simulation [10] utilize models like LSTM networks to predict discrepancies between simulation and real-world performance. However, these approaches often require large amounts of real-world data and are sensitive to noise, limiting their robustness.

Recent work has demonstrated the effectiveness of using real-world data to tune simulators, helping bridge the sim-to-real gap [11]. For instance, [12] propose a novel real-sim-real (RSR) transfer method. In the real-to-sim training phase, a task-relevant simulated environment is constructed using semantic information. A policy is then trained within this simulated environment. In the subsequent sim-to-real inference phase, the trained policy is directly applied to control the robot in real-world scenarios, without requiring any additional real-world data. Other methods, such as Bayessim [13], enhance domain randomization by incorporating real-world data to build a posterior distribution of simulation parameters. Additionally, [14] integrates vision-based foundation models with robotics tasks, enabling the reconstruction of robot poses from video using forward kinematics and gradient-based optimization techniques. Other than those methods, differentiable simulators [15] allow simulation parameters to be fine-tuned using gradient-based optimization techniques with real-world data. This enables the simulation environment to more closely match the real-world dynamics of the robot [16]. For example, [17] defines key physical parameters, such as mass and force control inputs, and uses a differentiable physics engine to simu-

late corresponding states. These simulated states are then compared with real-world data, such as video recordings, to generate a loss function. Backpropagation is applied to update the simulator parameters, improving the simulation’s accuracy. In another example, [18] establishes a full differentiable pipeline, linking pixel observations to reinforcement learning (RL) policies and state estimation, which significantly enhances RL performance.

However, these approaches face several challenges. First, many existing methods overlook potential biases in real-world data collection, which can lead to suboptimal tuning results. The assumption that real-world data accurately represents the robot’s domain may not always hold, especially if the data is collected in a non-representative manner or fails to cover the regions of interest for the policy. Second, some methods rely solely on visual appearance or video data for tuning. While this approach can provide useful information, it is highly sensitive to factors such as lighting conditions, camera angles, and sensor calibration, which require rigorous experimental setups. Additionally, visual data primarily captures information about the pose of the robot, but it often fails to provide insights into critical dynamic variables like velocity, acceleration, or thrust, which are essential for accurate simulation and control. Finally, many of these approaches are limited to specific types of robots or environments, reducing their generalizability.

To overcome these limitations, we propose a novel framework for sim-to-real transfer that leverages real-world data to adjust the parameters of a differentiable simulator. Our framework uses a cost function derived from information theory, which incorporates sim2real gap considerations and encourages the policy to collect data that is most informative for tuning the simulator. This cost function can be integrated with various reinforcement learning algorithms, such as PPO [19] and SAC [20], etc. In addition, we consider both physical states and visual appearance as part of the cost, enabling more comprehensive tuning. Our framework is built on the MuJoCo MJX engine [21], ensuring compatibility with a wide range of robotic platforms. We demonstrate the effectiveness of our approach through several experiments on a robotic arm. At the end of the paper, we present the discussion on the effect include the visual loss for the computation, limitation of the work and our future works.

II. PRELIMINARY

A. Reinforcement Learning Algorithms

Reinforcement Learning (RL) is a framework where an agent learns to make sequential decisions by interacting with an environment to maximize a cumulative reward. The agent observes the current state s_t at each time step t , selects an action a_t , and receives feedback in the form of a reward r_t . The goal is to learn a policy $\pi(a_t|s_t)$, which defines the probability distribution over actions a_t given a state s_t , that maximizes the expected cumulative reward.

The networks are usually trained using the following

objective:

$$\mathcal{L}_{task} = \mathbb{E}[(r_t + \gamma V(s_{t+1}) - V(s_t))\nabla_{\pi} \log \pi(a_t|s_t)] \quad (1)$$

The goal of training is to minimize this cost, thereby improving the value function and, consequently, the policy over time.

B. Differentiable Simulator

A differentiable physical engine allows the computation of gradients with respect to physical simulation parameters, e.g., friction, mass, and elasticity, etc., enabling optimization of those parameters. In a typical physics engine, the state of the system s_t evolves according to some physical laws, modeled as a function $f_{\theta}(s_t, a_t)$, where θ represents the system parameters, and a_t is the control input (action). The differential form of the system dynamics can be computed by applying the chain rule to the physical engine’s equations of motion. This gradient allows us to optimize the system’s parameters θ using standard gradient-based techniques.

C. Data Collection Approaches

Common methods for data collection [22] include random sampling, grid sampling, and trajectory-based sampling, etc. (1) In random sampling [23], data points are selected independently from the state space, often resulting in an uneven distribution that may not cover critical regions. Mathematically, if S represents the state space, random sampling involves selecting points $s_i \in S$ with uniform probability, which can lead to underrepresentation of important regions $S_{critical} \subset S$. (2) Grid sampling [24], where data points are chosen systematically over a predefined grid, ensures coverage of the state space but can suffer from high computational costs, particularly in high-dimensional environments. If the state space S is partitioned into N discrete regions, the number of samples grows as $O(N^d)$ for d -dimensional spaces, making this approach inefficient in large-scale settings. (3) Trajectory-based sampling collects data along the robot’s trajectories, but it often focuses disproportionately on regions the current policy already explores. Let \mathcal{T}_i denote the trajectory of the robot, and the data sampled along \mathcal{T}_i may over-represent regions $\mathcal{T}_i \subset S$ that the policy already visits, neglecting unexplored regions $S \setminus \mathcal{T}_i$.

D. Information Theory

Information theory provides fundamental tools for quantifying and comparing distributions of information [25]. If a particular data point or event significantly alters the distribution, it means that the data point is “informative” [26]. Here we give a short introduction to the basic concepts in the information theory that will be further used in the proposed structure.

1) *Kernel Density Estimation (KDE)*: Kernel Density Estimation [27] is a non-parametric way to estimate the probability density function of a random variable from a set of samples $\{D\}$. It smooths the distribution of data by placing a kernel (e.g., a Gaussian) on each data point and

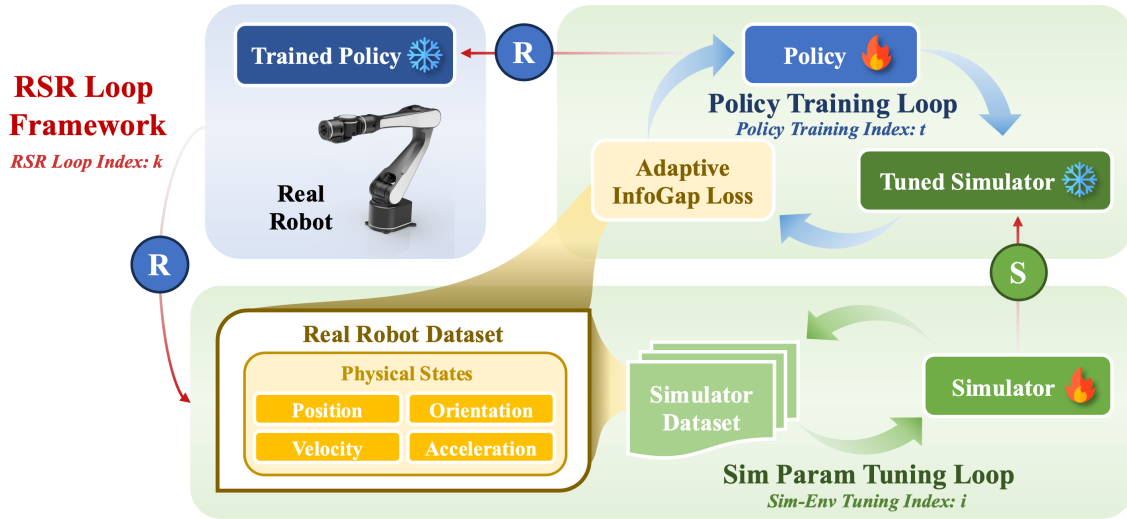


Fig. 1. Overview of the proposed RSR (Real-to-Sim-to-Real) Loop Framework (marked in red), consisting of two key feedback loops. The “Sim-Env Parameters Tuning Loop” (marked in green) adjusts the simulator parameters by utilizing data from the real robot. This loop iterates (indexed by i) to fine-tune the simulator, reducing the sim-to-real gap. The “Policy Training Loop” (marked in blue) utilized the tuned simulator of the current iteration k and the adaptive InfoGap loss to further train a policy for the next iteration. Together, these loops facilitate continuous improvement of both the policy and the simulator to enhance real-world performance.

summing these kernels to approximate the overall distribution. Mathematically, KDE is expressed as:

$$\hat{p}(\mathcal{D}) = \frac{1}{nh} \sum_{i=1}^n K\left(\frac{x - x_i}{h}\right)$$

where K is the kernel function, h is the bandwidth parameter that controls the smoothness, and $x_i \in \{\mathcal{D}\}$ are the data points.

2) *Distribution Divergence Measure*: The “Kullback-Leibler (KL) divergence” is a measure of how one probability distribution diverges from a second probability distribution. KL divergence is often used as a cost function to measure the dissimilarity between two distributions p and q :

$$\text{KL}(p \parallel q) = \sum_x p(x) \log\left(\frac{p(x)}{q(x)}\right)$$

The “Wasserstein distance”, also known as “Earth Mover’s Distance (EMD)”, is another metric used to measure the difference between two probability distributions. It is particularly useful in situations when the geometry of the space is important. The Wasserstein distance $W_\beta(p, q)$ of order β for two probability distributions p and q can be intuitively thought of as the minimum cost of transforming one distribution into another, where the cost is determined by the amount of mass moved and the distance it is moved.

III. METHOD

A. System Overview

In this section, we provide an introduction to the proposed structure as shown in Fig. 1. The goal is to collect real-world data from the robot to tune the simulator and construct the cost function for policy training, and then deploy the trained policy on the real robot to collect new data for the next

iteration. This iterative process is referred to as the “Real-Sim-Real (RSR) Loop Framework”, which aims to improve sim-to-real transfer. Through continuous cycles of environment tuning and policy training, the robot’s performance are progressively enhanced within limited iterations, resulting in a more robust system. In the following, we will outline the details of each key component of the proposed structure. The algorithm is illustrated in the Appendix VIII-A

B. Simulation-Env Parameter Tuning Process

To align the simulation environment with real-world dynamics, we iteratively optimize the simulation parameters θ using data collected from real-world experiments.

$$\theta = \arg \min \mathcal{L}_{\text{physical}}(\mathcal{D}_{\text{real}} - \mathcal{D}_{\text{sim}}(\theta)) \quad (2)$$

The optimization process minimizes the physical loss $\mathcal{L}_{\text{physical}}$, which is computed as the discrepancy between the real-world measurements $\mathcal{D}_{\text{real}}$ and their simulated counterparts $\mathcal{D}_{\text{sim}}(\theta)$. The total loss \mathcal{L} is then minimized using gradient-based optimization, where the parameters θ are updated as

$$\theta \leftarrow \theta - \alpha \nabla_{\theta} \mathcal{L}(\theta) .$$

Through backpropagation, this process adjusts the simulation parameters iteratively to ensure the environment accurately reproduces both the physical behaviors and visual appearances observed in real-world data.

C. Adaptive InfoGap Loss construction

Once the simulator is tuned for the current iteration, it is used to train the new policy. The trained policy is then deployed on the real robot to collect data for the next iteration, i.e., a trajectory-based sampling method is utilized as discussed in Sec. II-C. Thus, the cost function used for policy training must be designed not only to focus on task

completion but also to address the collection of new real-world data that helps narrow the sim-to-real gap. As noted earlier, trajectory-based sampling can introduce bias when estimating the distribution of the real-world domain. To mitigate this, we balance the estimation of the real domain with task completion throughout the iterations, ensuring that the policy explores underrepresented regions of the real world while still optimizing for task performance.

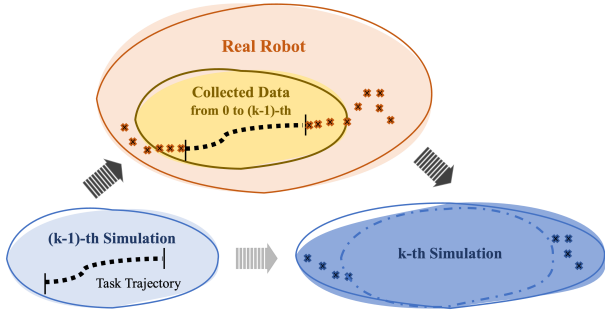


Fig. 2. The process of bridging the sim-to-real gap in robot training. When the discrepancy between the simulation (blue domain) and real robot (orange domain) is large, the policy prioritizes collecting informative data (marked as crosses) from the real domain to better characterize its properties other than the task trajectory (black dashed line).

The core idea as shown in Fig. 2 is that when the discrepancy between the simulation environment and the real robot is substantial, the policy prioritizes collecting more informative data that better characterizes the real domain properties rather than focusing solely on task completion. This is because a policy trained under such a significant sim-to-real gap is unlikely to perform well on the real robot. As the gap narrows and the simulator parameters converge towards the real domain, this term in the loss function diminishes, allowing the policy to shift its focus to task completion.

Specifically, this adaptive InfoGap cost and the corresponding minimization problem to determine the action at timestep t during the k -th sim-to-real tuning iteration is constructed as

$$a_{k,t} = \arg \min \mathcal{L}(a_{k,t}) = \mathcal{L}_{task}(a_t) + \mathcal{L}_{sr}(a_{k,t}) ,$$

where \mathcal{L}_{task} is the nominal cost (1) for task completion and

$$\mathcal{L}_{sr} = -\text{KL}(\hat{p}(\mathcal{D}_{real}^k) \parallel \hat{p}(\mathcal{D}_{sim}^{k-1})) \cdot W_{\beta}(\hat{p}(\mathcal{D}_{sim}^k + \mathcal{D}_t), \hat{p}(\mathcal{D}_{sim}^k)) . \quad (3)$$

The meanings of each notation are:

- \mathcal{D}_{real}^k : the data set of length M $\{s_m, a_m = \pi_{k-1}(s_m), s_{m+1}^{real}\}_0^M$ collected from the actual robot with the policy π_{k-1} trained from the last iteration $k-1$.
- \mathcal{D}_{sim}^{k-1} : the data set of the same input but propagated in the untuned simulator $\{s_m, a_m, s_{m+1}^{sim}\}_0^M$.
- \mathcal{D}_{sim}^k : the dataset propagated in this tuned new simulator $\{s_m, a_m, \hat{s}_{m+1}^{sim}\}_0^M$.
- \mathcal{D}_t : the data pair generated by the current input $a_{k,t}$.
- $\hat{p}(\{\mathcal{D}\})$ represents the distribution estimation function from data samples set \mathcal{D} .

- $\text{KL}(p, q)$ and W_{β} represents the KL divergence and Wasserstein distance, separately.

At the beginning of each training iteration k in the simulation, the first term, $\text{KL}(\hat{p}(\mathcal{D}_{real}^k) \parallel \hat{p}(\mathcal{D}_{sim}^{k-1}))$, remains constant throughout the training process and represents the sim-to-real gap at the current iteration. Meanwhile, a specific data pair \mathcal{D}_t , influenced by the policy’s action a_t during training, affects the second term, $W_{\beta}(\hat{p}(\mathcal{D}_{sim}^k + \mathcal{D}_t), \hat{p}(\mathcal{D}_{sim}^k))$. This term encourages the policy to generate actions that produce more informative data—data that exhibit larger discrepancies from the simulated distribution while being closer to the real-world distribution. Therefore, the cost function is designed to encourage actions that are more informative and exploratory, enabling the collection of data that fully captures the distribution or characteristics of the real domain, thereby mitigating data bias when addressing the sim-to-real gap. When the sim-to-real gap becomes negligible (i.e., $\text{KL}(\hat{p}(\mathcal{D}_{real}^k) \parallel \hat{p}(\mathcal{D}_{sim}^{k-1}))$ approaches zero), this term \mathcal{L}_{sr} in the cost function diminishes, leaving only the task completion cost \mathcal{L}_{task} to guide the actions. Ultimately, this approach yields a policy capable of completing the task effectively while minimizing the sim-to-real gap.

IV. EXPERIMENTS

In this section, we present a series of experiments designed to evaluate and validate the effectiveness of our proposed RSR loop framework in the block-pushing tasks with a 6-dof robotic arm.

A. Experimental Settings

For the simulation, we use the DISCOVERSE [28] simulator to model the robot’s interactions with its environment. The reinforcement learning algorithm used is PPO, implemented with the JAX computation library. Definitions of action space, observation space and rewards used in the RL policy are shown in Appendix VIII-B. The simulation runs on a laptop equipped with an NVIDIA 4090 GPU and 24GB of memory. In the real-world experiments, a 6-DOF AIRBOT Play robotic arm is used to execute object manipulation tasks. The robot is equipped with a Realsense D435i depth camera for visual perception, providing accurate pose estimation of the objects in the workspace.

B. Block Pushing Experiment

In this experiment, the robot is required to push the block to random target points within the workspace. We trained the policy in the original simulation (marked as “simulated trajectory”), transferred it to the real robot (marked as “1st PPO”), and iterated through the n -th RSR loop to obtain the corresponding trajectories in the real environment (marked as n -th RSR Trajectory). As seen in Table I, the KL divergence between the simulation and real trajectories is initially high, particularly in the 1-st PPO stage. This indicates a significant discrepancy between the simulation-trained policy and the real-world environment. However, after applying multiple iterations of the RSR loop, the KL divergence progressively decreases, demonstrating that the simulator is

becoming more representative of real-world dynamics, and the refined policy is better aligned with real-world behavior. This demonstrates the effectiveness of the designed InfoGap loss.

TABLE I
RESULTS OF DISTRIBUTION DEVIATION

| Stage | KL Divergence (X) | KL Divergence (Y) |
|---------|-------------------|-------------------|
| 1st_PPO | 16.3509 | 36.3168 |
| 2nd_RSR | 1.6903 | 3.4206 |
| 3rd_RSR | 5.0462 | 2.3946 |
| 4th_RSR | 0.9739 | 0.8384 |

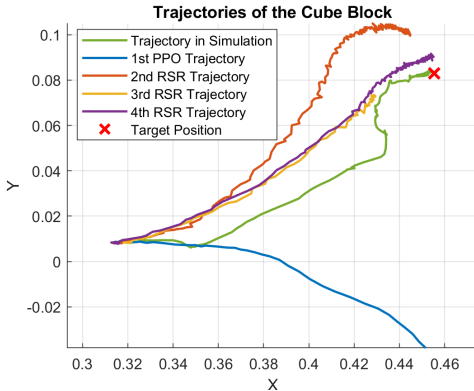


Fig. 3. Real-world pushing trajectories across different iterations.

The improvement in trajectory alignment is further visualized in Fig. 3, which shows the block’s trajectories at different training stages. The 1st PPO trajectory (blue) deviates significantly from the simulation trajectory and fails to reach the target. The low friction between the cube and the desk as well as the misalignment between the gripper and the cube causes the gripper to slip along the cube’s surface instead of effectively pushing it, resulting in the cube moving in an unintended direction. In contrast, the RSR-refined trajectories (orange, yellow, and purple) show a progressive improvement in accuracy. By the 4th RSR iteration (purple), the real-world trajectory closely matches the simulation trajectory, and the block successfully reaches the target position (red cross “x”). These results highlight the effectiveness of the RSR approach in closing the sim-to-real gap. By iteratively refining the simulation model and retraining the policy, we achieve a substantial reduction in trajectory divergence and significantly improve the real-world task performance. To ensure the reliability of our results and mitigate potential biases, we repeated the experiments three times. Fig. 4 presents the mean trajectory error in both the X and Y directions over time, computed as the deviation of real-world trajectories from the simulation reference, averaged over three independent runs. The error trends illustrate how the RSR framework progressively refines the simulation parameters, leading to improved alignment between simulated and real trajectories with similar patterns of error reduction that are observed in Fig. 3, further supporting the effectiveness of our approach in bridging the sim-to-real gap.

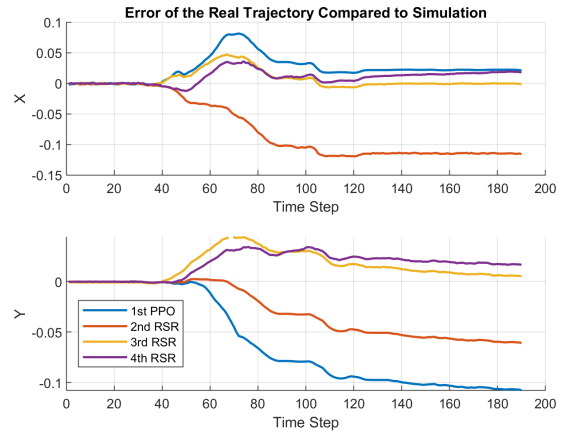


Fig. 4. Mean trajectory error over three trials in the X and Y directions against time for different iterations.

C. T-shaped Block Pushing

In this variant of the block-pushing task, the robot is required to push a T-shaped object to a specified target position. This experiment provides a more challenging scenario due to the object’s geometry and the increased difficulty of manipulating irregularly shaped objects. We did the similar experiments as we evaluated in the cube block. Three trials were conducted and the results are shown in Fig. 5. The figure shows the yaw error decreasing as the RSR iterations progress. The initial PPO policy (blue) has a high yaw error, while the 2nd RSR iteration (red) starts improving but remains unstable. By the 3rd (yellow) and 4th (purple) iterations, the error is significantly reduced, demonstrating the effectiveness of the RSR pipeline in refining sim-to-real alignment. The similar performance validates the efficiency of the proposed pipeline in different types of tasks.

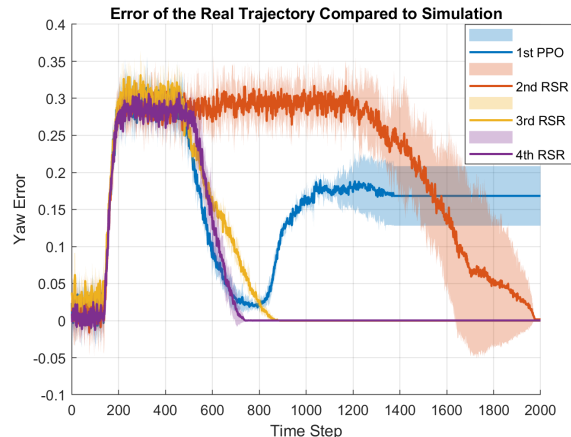


Fig. 5. 1- σ bounds of real trajectories for the yaw angle in the T-shaped block pushing trials for different iterations, where the shaded area represents the bounds.

V. DISCUSSION ON INCORPORATING VISUAL LOSS

In our experiments, we explored the possibility of incorporating a visual loss component into the sim-to-real adaptation

process. Specifically, we computed the visual loss using the Structural Similarity Index (SSIM [29]) between Gaussian-rendered simulation images and real-world images. This loss was then used as a multiplier to the original sim-to-real loss, aiming to improve domain alignment by encouraging the simulator to produce not only physically but also visually consistent data.

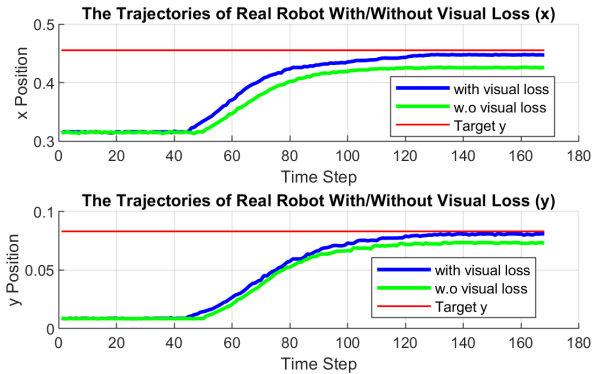


Fig. 6. Trajectories of real-robot deployment with and without visual loss.

However, as shown in Fig. 6, the results indicate that incorporating the visual loss in this manner does not lead to improved performance. In fact, it appears to introduce instability in the adaptation process. One possible reason for this is that while SSIM effectively captures high-level structural similarity, it does not directly correlate with the physical parameters that affect policy learning. As a result, using SSIM-based visual loss as a weight may amplify discrepancies in ways that are not meaningful for improving real-world task performance. Additionally, since the visual differences can be caused by lighting conditions, reflections, and camera noise—factors that do not directly impact the underlying dynamics—forcing the simulator to match real images too closely might introduce misleading optimization directions.

Another critical limitation we observed is the computational cost associated with rendering high-fidelity images for environment parameter tuning. Real-time rendering with physically realistic lighting and textures requires significant GPU resources, making it impractical for iterative training. Given these challenges, we have chosen not to include the visual loss in our current pipeline. Instead, our approach primarily focuses on optimizing the physical parameters that directly affect sim-to-real transfer.

VI. LIMITATIONS

While the RSR framework demonstrates promising results in bridging the sim-to-real gap, there are certain limitations that need to be addressed in future research and development. Firstly, the speed of the overall algorithm is heavily dependent on the underlying simulation engine (MuJoCo MJX) and the computation framework (JAX). While MJX offers a highly accurate and flexible simulation environment, it requires massive computational resources.

On the other hand, in this study we have primarily focused on environmental effects that can be explicitly tuned, such as friction, mass, and elasticity, etc. While these effects are important for sim-to-real transfer, they only represent a subset of the factors that influence the real-world performance of robotic systems. The RSR framework’s current implementation does not account for implicit environmental factors, such as dynamic ground effects or other non-observable environmental variables that may require adjustments at the physical level. In future experiments, we are trying to extend our framework to aerial robots. The dynamics of aerial robots are fundamentally different from ground robots, as they are subject to various environmental effects such as wind, atmospheric pressure, and turbulence.

VII. CONCLUSION AND FUTURE WORK

In this work, we propose an RSR pipeline to facilitate smoother sim-to-real transfer by leveraging real-world data through two key components: a gap-aware loss function that can be integrated into standard reinforcement learning methods and a parameter tuning process for a differentiable simulator. The approach is evaluated using a 6-DOF robotic arm. Experimental results demonstrate that the proposed loss function effectively reduces the divergence between simulation and reality while improving the performance of simulator-trained policies in real-world deployment through iterative RSR refinements.

This work makes a significant contribution to the development of a more robust and efficient pipeline for transferring policies learned in simulation to real robots, advancing the state of the art in sim2real research. Note that the proposed structure is also highly adaptable and can be applied in a general policy transfer scenario, provided that data from the target environment can be collected. This opens up new possibilities for autonomous robots to learn and operate in diverse, previously unexplored environments with minimal additional training, making it a versatile tool for a wide range of robotic applications.

Future work will focus on testing the RSR framework with aerial robots, where the effects of the environment—such as wind resistance, ground effects, and turbulence—will be accounted for by implicitly adjusting simulation parameters. We also aim to improve the framework’s ability to adapt to these dynamic environmental changes during the real-time execution of the task.

REFERENCES

- [1] T. Goyal, S. Hussain, E. Martinez-Marroquin, N. A. T. Brown, and P. K. Jamwal, “Stiffness-observer-based adaptive control of an intrinsically compliant parallel wrist rehabilitation robot,” *IEEE Transactions on Human-Machine Systems*, vol. 53, no. 1, pp. 65–74, 2023.
- [2] S. Höfer, K. Bekris, A. Handa, J. C. Gamboa, M. Mozifian, F. Golemo, C. Atkeson, D. Fox, K. Goldberg, J. Leonard, *et al.*, “Sim2real in robotics and automation: Applications and challenges,” *IEEE transactions on automation science and engineering*, vol. 18, no. 2, pp. 398–400, 2021.
- [3] H. Ge, R. Wang, Z.-a. Xu, H. Zhu, R. Deng, Y. Dong, Z. Pang, G. Zhou, J. Zhang, and L. Shi, “Bridging the resource gap: Deploying advanced imitation learning models onto affordable embedded platforms,” *IEEE International Conference on Robotics and Biomimetics (ROBIO)*, 2024.

- [4] E. Salvato, G. Fenu, E. Medvet, and F. A. Pellegrino, “Crossing the reality gap: A survey on sim-to-real transferability of robot controllers in reinforcement learning,” *IEEE Access*, vol. 9, pp. 153 171–153 187, 2021.
- [5] W. Zhao, J. P. Queralta, and T. Westerlund, “Sim-to-real transfer in deep reinforcement learning for robotics: A survey,” in *IEEE symposium series on computational intelligence (SSCI)*, 2020, pp. 737–744.
- [6] J. Tobin, R. Fong, A. Ray, J. Schneider, W. Zaremba, and P. Abbeel, “Domain randomization for transferring deep neural networks from simulation to the real world,” in *IEEE/RSJ international conference on intelligent robots and systems (IROS)*, 2017, pp. 23–30.
- [7] K. Bousmalis, A. Irpan, P. Wohlhart, Y. Bai, M. Kelcey, M. Kalakrishnan, L. Downs, J. Ibarz, P. Pastor, K. Konolige, et al., “Using simulation and domain adaptation to improve efficiency of deep robotic grasping,” in *IEEE international conference on robotics and automation (ICRA)*, 2018, pp. 4243–4250.
- [8] Y. Ganin, E. Ustinova, H. Ajakan, P. Germain, H. Larochelle, F. Laviolette, M. March, and V. Lempitsky, “Domain-adversarial training of neural networks,” *Journal of machine learning research*, vol. 17, no. 59, pp. 1–35, 2016.
- [9] K. Bousmalis, G. Trigeorgis, N. Silberman, D. Krishnan, and D. Erhan, “Domain separation networks,” *Advances in neural information processing systems*, vol. 29, 2016.
- [10] F. Golemo, A. A. Taiga, A. Courville, and P.-Y. Oudeyer, “Sim-to-real transfer with neural-augmented robot simulation,” in *Conference on Robot Learning*. PMLR, 2018, pp. 817–828.
- [11] E. Heiden, D. Millard, E. Coumans, Y. Sheng, and G. S. Sukhatme, “Neuralsim: Augmenting differentiable simulators with neural networks,” in *IEEE International Conference on Robotics and Automation (ICRA)*, 2021, pp. 9474–9481.
- [12] N. Liu, Y. Cai, T. Lu, R. Wang, and S. Wang, “Real–sim–real transfer for real-world robot control policy learning with deep reinforcement learning,” *Applied Sciences*, vol. 10, no. 5, p. 1555, 2020.
- [13] F. Ramos, R. C. Possas, and D. Fox, “Bayessim: Adaptive domain randomization via probabilistic inference for robotics simulators,” *arXiv preprint arXiv:1906.01728*, 2019.
- [14] R. Liu, A. Canberk, S. Song, and C. Vondrick, “Differentiable robot rendering,” in *8th Annual Conference on Robot Learning*, 2024.
- [15] R. Newbury, J. Collins, K. He, J. Pan, I. Posner, D. Howard, and A. Cosgun, “A review of differentiable simulators,” *IEEE Access*, 2024.
- [16] Y.-L. Qiao, J. Liang, V. Koltun, and M. C. Lin, “Efficient differentiable simulation of articulated bodies,” in *International Conference on Machine Learning*. PMLR, 2021, pp. 8661–8671.
- [17] J. K. Murthy, M. Macklin, F. Golemo, V. Voleti, L. Petrini, M. Weiss, B. Considine, J. Parent-Lévesque, K. Xie, K. Erleben, et al., “gradsim: Differentiable simulation for system identification and visuomotor control,” in *International conference on learning representations*, 2020.
- [18] J. Heeg, Y. Song, and D. Scaramuzza, “Learning quadrotor control from visual features using differentiable simulation,” *arXiv preprint arXiv:2410.15979*, 2024.
- [19] H. Xu, Z. Yan, J. Xuan, G. Zhang, and J. Lu, “Improving proximal policy optimization with alpha divergence,” *Neurocomputing*, vol. 534, pp. 94–105, 2023.
- [20] C. Xu, J. Ma, and H. Tao, “Batch process control based on reinforcement learning with segmented prioritized experience replay,” *Measurement Science and Technology*, vol. 35, no. 5, p. 056202, 2024.
- [21] C. Liao, Y. Wang, X. Ding, Y. Ren, X. Duan, and J. He, “Performance comparison of typical physics engines using robot models with multiple joints,” *IEEE Robotics and Automation Letters*, vol. 8, no. 11, pp. 7520–7526, 2023.
- [22] N. L. Leech and C. Donovan, *Mixed methods sampling and data collection*. International Encyclopedia of Education, 2023.
- [23] A. Kumar, A. S. Siddiqui, M. S. Mustafa, E. Hussam, H. M. Aljohani, and F. A. Almulhim, “Mean estimation using an efficient class of estimators based on simple random sampling: Simulation and applications,” *Alexandria Engineering Journal*, vol. 91, pp. 197–203, 2024.
- [24] S. R. Lindemann, A. Yershova, and S. M. LaValle, “Incremental grid sampling strategies in robotics,” in *Algorithmic Foundations of Robotics VI*. Springer, 2005, pp. 313–328.
- [25] R. B. Ash, *Information theory*. Courier Corporation, 2012.
- [26] J. Gao, Z. Wang, T. Jin, J. Cheng, Z. Lei, and S. Gao, “Information gain ratio-based subfeature grouping empowers particle swarm optimization for feature selection,” *Knowledge-Based Systems*, vol. 286, p. 111380, 2024.
- [27] Y.-C. Chen, “A tutorial on kernel density estimation and recent advances,” *Biostatistics & Epidemiology*, vol. 1, no. 1, pp. 161–187, 2017.
- [28] Y. Jia, G. Wang, Y. Dong, J. Wu, Y. Zeng, H. Ge, K. Ding, Z. Yan, W. Gu, C. Li, Z. Wang, Y. Cheng, W. Sui, R. Huang, and G. Zhou, “DISCOVERSE: Efficient robot simulation in complex high-fidelity environments,” 2024. [Online]. Available: <https://air-discoverse.github.io/>
- [29] U. Sara, M. Akter, and M. S. Uddin, “Image quality assessment through FSIM, SSIM, MSE and PSNR—a comparative study,” *Journal of Computer and Communications*, vol. 7, no. 3, pp. 8–18, 2019.

VIII. APPENDIX

A. Algorithm

The whole framework can be illustrated as in the following algorithm:

Algorithm 1 The RSR Loop Framework

- 1: **Initialize:** Initial policy π_0 , environment parameters θ_0 , and initial real dataset \mathcal{D}_{real}^0 collected from the deployment of π_0 on the real robot.
- 2: **while** not converged, at iteration k **do**
- 3: **Step 1: Environment Parameter Tuning**
- 4: Initialize $\theta_{i=0,k-1} = \theta_{k-1}$, compute the corresponding loss function $\mathcal{L}(\theta_{i,k-1})$ for each parameter $\theta_{i,k-1}$ with the new real dataset \mathcal{D}_{real}^k . Update the environment parameters $\theta_{i,k-1}$ using gradient descent

$$\theta_{i,k-1} \leftarrow \theta_{i-1,k-1} - \alpha \nabla_{\theta} \mathcal{L}(\theta_{i-1,k-1})$$

until they converge and assign $\theta_k = \theta_{i,k-1}$ to settle down the simulation environment of the current iteration.

- 5: **Step 2: Policy Training**
- 6: Using the updated environment θ_k , perform reinforcement learning training for the policy π_k with the adaptive InfoGap cost 3 included:

$$\mathcal{L}(\pi_k) = \mathbb{E}_{s_t, a_t \sim \pi_k} [r_t + \gamma \mathbb{V}_{\pi_k}(s_{t+1}) - \mathbb{V}_{\pi_k}(s_t)] + \mathcal{L}_{sr}^k$$
- 7: **Step 3:** Deploy the updated policy π_k on the real robot and collect new real-world data \mathcal{D}_{real}^{k+1} . Repeat the process for subsequent iterations.

8: **end while**

B. RL Settings

Action Space: The action space is parameterized as a 6-dimensional vector governing the rotational displacements of individual robotic joints, optimized for articulated control precision in Cartesian space operations.

Observation Space: The observation space for the cube-block pushing experiment consists of a 6-dimensional vector representing joint angles, the Cartesian coordinates of the end-effector, a 3-dimensional vector for the target position, and a 3-dimensional vector for the block position, along with their relative displacement vectors. For the T-shaped block pushing task, the observation space is augmented to include

both position and orientation, incorporating quaternion representations for the target and block poses.

Reward Setup:

- (1) **Cube Block Experiment** The total reward function consists of two components. Firstly, the distance-based reward r_d encourages the block to reach the target position: $r_d = -\|\mathbf{x}_b - \mathbf{x}_t\|_2$, where $\|\cdot\|_2$ represents the Euclidean norm. Secondly, the end-effector guidance reward r_{ee} , encourages the manipulator to move towards the block: $r_{ee} = -\|\mathbf{x}_{ee} - \mathbf{x}_b\|_2$. The total reward is given by: $r = \lambda_d r_d + \lambda_{ee} r_{ee}$, where λ_d, λ_{ee} are weighting coefficients, which is [6.0, 3.0] in this test.
- (2) **T-shaped Block Experiment** The reward function for manipulating the T-shaped block includes both position and orientation components that is $r = \lambda_d r_d + \lambda_o r_o$, where the orientation reward r_o penalizes deviations from the desired orientation: $r_o = -\arccos(\langle \mathbf{q}_b, \mathbf{q}_t \rangle)$ that $\langle \mathbf{q}_b, \mathbf{q}_t \rangle$ represents the inner product of the unit quaternions, measuring the angular difference. λ_d and λ_o are weighting coefficients ensuring proper balance between positional and orientation alignment, which is [3.0, 6.0] in this test.